Langmuir

Article

pubs.acs.org/Langmuir

Rod Hydrodynamics and Length Distributions of Single-Wall Carbon Nanotubes Using Analytical Ultracentrifugation

Carlos A. Silvera Batista, Ming Zheng, Constantine Y. Khripin, Xiaomin Tu, and Jeffrey A. Fagan*

Materials Science and Engineering Division, National Institute of Standards and Technology, 100 Bureau Drive, Gaithersburg, Maryland 20899, United States

Supporting Information

ABSTRACT: Because of their repetitive chemical structure, extreme rigidity, and the separability of populations with varying aspect ratio, SWCNTs are excellent candidates for use as model rodlike colloids. In this contribution, the sedimentation velocities of length and density sorted single-wall carbon nanotubes (SWCNTs) are compared to predictions from rod hydrodynamic theories of increasing complexity over a range of aspect ratios from <50 to >400. Independently measuring all contributions to the sedimentation velocity besides the shape factor, excellent agreement is found between the experimental findings and theoretical predictions for numerically calculated hydrodynamic radius values and for multiterm analytical expansion approximations; values for the hydrodynamic radii in these cases are additionally found to be consistent with the apparent hydrated particle radius determined independently by buoyancy measurements. Lastly, we utilize this equivalency to calculate the apparent distribution of nanotube lengths in each population from their sedimentation coefficient distribution without adjustable parameters, achieving excellent agreement with distributions from atomic force microscopy. The method developed herein provides an alternative for the ensemble measurement of SWCNT length distributions and others rodlike particles.

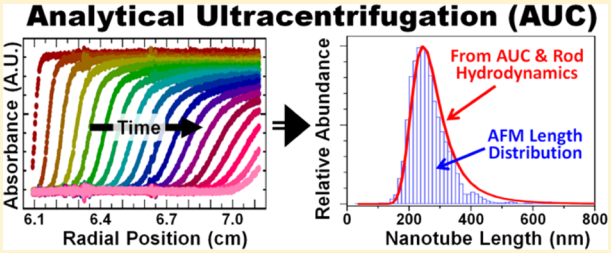

INTRODUCTION

Measurements for the size of dispersed colloidal or nanoscale particles in solution typically rely on expressions relating the motion of the particles to their size, with a caveat that the shape of the dispersed particles strongly affects the particle motion and thus must be incorporated into the hydrodynamic analysis to achieve accurate sizing. Theoretical approximations describing the hydrodynamic effects of particle shape have been extensively developed since the 1920s for simple anisotropic particles, in particular for 1-D nonspherical particles such as ellipsoids or cylinders.[1] This is due to the interest in, and tractability of, their solution dynamics, importance to fields such as biology (e.g., DNA), and effects on phenomena such as self-assembly.[2] For rodlike particles, with L and d as the length and diameter, shape effects are generally collected into an effective friction coefficient that is a function of the aspect ratio (L/d). Broad comparison of the theoretical descriptions with experimental values, however, has strikingly lagged behind the development of the theory for rodlike systems, which leaves doubt that a rod particle can be accurately sized by the use of those descriptions. This lag, and hence uncertainty, is directly traceable to a lack of appropriate model particle systems that fulfill all of the requirements for an ideal rodlike particle and extend to aspect ratios $\gg$20; ideal rod particles would be straight and rigid, small enough to satisfy flow field assumptions during sedimentation, stable in dispersion, and variable in aspect ratio over a broad range.[3,4]

In this work, single-wall carbon nanotubes (SWCNTs) are used as model rodlike particles to experimentally compare against expressions for the friction coefficient that result from both slender body theory[5] and numerical methods, including path-integration[6] and boundary element methods, with the best models then used to calculate the length distribution of individual fractions for comparison to counting techniques.[7] SWCNTs are an exceptional class of nanomaterial that are ideal model particles for experimental rod hydrodynamics validation. For each species of SWCNT (defined by the roll-up vector or chirality) the carbon-center to carbon-center diameter is known and is uniform along the axis of the nanotube. Varying the length of the SWCNT (length populations from a few nanometers to several micrometers can be separated from a polydisperse parent population with current technologies) thus produces samples in which only the aspect ratio is changed,[8] and because the diameter is constant, properties such as the buoyant density are length independent. Moreover, under proper dispersion conditions, SWCNT dispersions are stable for months to years without settling or agglomeration. Finally, the reported persistence lengths of SWCNTs are on the order of 10−100 μm and scale with d^3 such that larger diameter SWCNTs (like those used here) are stiffer.[9,10] This indicates that SWCNTs can reasonably be considered rigid rods from a

Received: December 30, 2013
Revised: February 28, 2014
Published: April 8, 2014

theoretical point of view over a broad range of aspect ratios, and experimental measurements on SWCNTs have shown on average that this scaling is valid through methods such as small-angle neutron scattering experiments.[11,12]

Although other particles with controlled shape and aspect ratios[3,4,13] have previously been measured for comparison to rod hydrodynamic theories, no other system has provided the wide range of aspect ratio variation while holding all other important parameters constant that SWCNTs provide. For example, previous experimental works measuring the friction coefficient of rodlike particles have been limited to aspect ratios that were either small or confined to a narrow range. Tirado et al. studied DNA strands of increasing length to compare experimental results against theoretical values of the sedimentation coefficient.[14] However, the aspect ratio range of that study was limited to values of less than ≈20 because DNA strands with more than 160 base pairs became semiflexible. Similar limitations, but for synthesis reasons, occur for stretched latex and gold nanorods,[15,16] which rarely exceed aspect ratios of ≈10 and are difficult to obtain with invariant diameter values even over that narrow range. Lastly, more promising effectively rodlike particles such as the fd virus, tobacco mosaic viruses (TMV), boehmite, and imogolite[13,17−19] also have limitations for broad investigations, including unknown or inaccurate values of density, discrete and invariable particle length, surface inhomogeneity, significant flexibility (i.e., short persistence lengths), and sample scarcity due to the high cost of systematic synthesis/molecular engineering.[20−22]

In this work we use analytical ultracentrifugation (AUC) to access the hydrodynamic behavior of a broad range of SWCNT aspect ratios, in different samples, through measurement of the sedimentation velocity. Using other, independently measured, information such as the density of the solvated SWCNTs and the length distribution of a population, the sedimentation velocity can be directly compared to the theoretical predictions for the effective friction coefficient as a function of length without any adjustable parameters. We can thus validate for nanotubes the predictions from hydrodynamic theory with experimental data.

In AUC as we implement it here (sedimentation velocity mode), the concentration distribution of a large ensemble of initially uniformly distributed particles is tracked with time as they sediment under centrifugal acceleration. The speed and shape of the sedimentation boundary, resulting from the depletion of particles near the meniscus as they move toward the outer radius, depend on the size and shape, as well as the density, of the particles. As a concurrent fractionation and characterization technique, AUC allows resolution of size and/or density distributions in a single experiment with high resolution.[23] Ultimately, if additional information is known, a measured distribution of sedimentation coefficients can be further transformed directly into molecular weight distributions or, as demonstrated herein, the length distribution of the SWCNTs present in the sample. The demonstrated use here of AUC to measure the length distributions is a significant accomplishment on its own merits. Previous studies have measured length distributions by tracking individual SWCNTs using single particle fluorescence microscopy[24] or measurements of alignment under shear flow.[25] However, defective, kinked, or short tubes are difficult to image through fluorescence, and particle tracking in constrained volumes requires approximated corrections for wall effects that intrinsically make difficult the use of the data for the verification of hydrodynamic models.[24,26] For the validation of the hydrodynamic models in this study, the length distribution for each population were thus determined independently of the sedimentation experiments through exhaustive imaging (>500 SWCNTs/fraction) of each aspect ratio sample using an atomic force microscope (AFM). This however is tedious, and consequently, the ability to extract length distributions from sedimentation data as demonstrated at the end of this contribution has significant value, as well as the advantages of measuring a much large number of particles and measuring them in their native dispersed state.

Therefore, herein, friction coefficients of two distinct diameter populations of rigorously prepared, length-sorted SWCNTs in dilute suspension are extracted from sedimentation velocity experiments performed in an analytical ultracentrifuge and quantitatively compared to predictions from hydrodynamic models. Similarly, a general strategy is developed and shown to extract length distributions from sedimentation velocity data.

METHODS

Preparation of Suspensions and Sorting of SWCNTs. SWCNTs produced through arc discharge (Batch AP-301, Carbon Solutions, Inc.,[27] and laser ablation (NASA-JSC soot #339) methods were first dispersed in an aqueous solution containing 20 g/L sodium deoxycholate (DOC) surfactant (BioXtra, >98%, Sigma). Dispersion processing consisted of sonication for 30 min ≅ 1 W/mL of applied power (tip sonicator, 0.64 cm, Thomas Scientific) of the SWCNT powder loaded at 1 mg/mL in the 20 g/L surfactant solution. To avoid excessive heating during sonication, the samples were immersed in an ice bath. Postsonication, large aggregates and heavy impurities were removed through centrifugation (2 h in a Beckman JA-20 rotor at 1885 rad/s (18 000 rpm)), after which the resulting supernatant was carefully decanted and saved.

Separation of empty and filled SWCNTs was performed following a procedure adapted from ref 28. Separation at high applied centrifugal acceleration was performed in a Beckman VTi 50 rotor along with OptiSeal tubes at 50 000 rpm for 3.5 h and 20 °C. A three-layer density column was used for this separation: the 7.5 mL bottom layer consisted of 15% (mass/volume) iodixanol (sold as OptiPrep, Aldrich) and 10 g/L DOC; the middle layer consisted of 22 mL of either 9% iodixanol (Laser-SWCNTs) or 10% iodixanol (Arc-SWCNTs) with 10 g/L DOC; the top layer (≈7 mL) was composed of the SWCNT suspension supernatant in 20 g/L DOC from the initial purification. Separation of the empty and water-filled SWCNTs occurs during the centrifugation due to the disparate average density differences of the two populations to the race layer density. This difference is directly reflected in the velocities of the two populations, which leads to spatial separation. Postseparation, samples containing the same fraction from multiple tubes/runs were combined, concentrated using forced membrane filtration, and dialyzed via repeated concentration-dilution steps to remove all of the iodixanol prior to the optical characterization. Figure S1 shows photos of one experiment before and after separation.

SWCNTs were sorted by length using a size-exclusion chromatography (SEC) procedure recently published by Khripin et al.,[8] which extended that technique to surfactant-dispersed SWCNTs. A GE ÄKTA Purifier HPLC system in conjunction with SEC columns packed with 5 μm silica-based beads were used for the fractionation. These columns (SEC-CNT) were purchased from Sepax Technologies Inc., Newark, DE. Three columns with pore size of 2000, 1000, and 300 Å were used in series, with a flow rate of 4 mL/min, and a injection volume of 2 mL of SWCNT dispersion. The samples were eluted with 10 g/L DOC. Fractions of 5 mL were collected.

Characterization of SWCNTs. UV−vis−NIR spectrometry was carried out on a Varian Cary 5000 spectrophotometer using a cuvette

dx.doi.org/10.1021/la404892k | Langmuir 2014, 30, 4895−4904

with either a 1 or 2 mm path length. The spectra of the reference 10 g/L DOC solution was acquired separately and linearly subtracted to yield the presented spectra representing only the absorbance for the SWCNTs in the dispersion.

For characterization with atomic force microscopy (AFM), silicon wafers functionalized with 3-(ethoxydimethylsilyl)propylamine (APDMES, Sigma-Aldrich, St. Louis, MO)[8] were used as substrates. The functionalization process consisted of first cleaning the substrates in a UV-O chamber for 15 min, followed by immersion into 1% APDMES in isopropanol for 20 min, followed by rinsing with isopropanol and DI water. Lastly, the wafers were dried in an oven at 70 °C for 20 min. Before deposition on the substrate, SWCNT samples in 10 g/L DOC were diluted at least 100× with an aqueous solution of 0.2% SC and 20 mM NaSCN. A concentration of DOC above 0.01% was found to interfere with the deposition of SWCNTs. In cases where the concentration of SWCNTs was too low after dilution for effective deposition, the samples were concentrated using 500 μL centrifugal filtration devices. SWCNTs were deposited onto the functionalized wafers by casting 5−20 μL of the sample, followed by incubation in a closed container for 8 min. After incubation, samples were blown dry using nitrogen. AFM imaging was done on a Bruker Dimension Icon AFM in the peak-force tapping mode (ScanAsyst) using the respective ScanAsyst-Air probes.

AUC Measurements. Analytical ultracentrifugation was performed on a Beckman-Coulter XL-I analytical ultracentrifuge in an AN-50 8 cell rotor with 2-sector Epon-charcoal centerpieces. The optical path length of these cells is 12 mm. Data were collected in sedimentation velocity mode with both the interference optics and absorption optics at centrifugation speeds of 733 rad/s (7000 rpm), 1466 rad/s (14 000 rpm), 2617 rad/s (25 krpm), 2932 rad/s (28 krpm), and 4188 rad/s (40 000 rpm) at 20 °C; most data were collected at 2617 rad/s. Although the calculated *Re* and rotational *Pe* numbers were small (discussed in detail later), alignment effects (of the nanotubes) were tested for by performing experiments at all the speeds mentioned above for fractions F4, F5, and F9 of the laser and arc samples. The peak values of the sedimentation coefficient distributions were invariant with the centrifugation speeds while the distributions overall showed marginal variations. Hence, alignment effects were considered insignificant.

SWCNT dispersions for AUC measurement were diluted with either H_2O−DOC, D_2O−DOC, or H_2O−iodixanol−DOC solutions to reach the desired concentration using a pipettor at a single fixed volume. For the experiments measuring the effects of the SWCNT aspect ratio only water solutions with 10 g/L DOC was used for dilution. Dilution ratios varied from 0 to 5× to reach an appropriate concentration yielding an absorbance of ≈0.8 at the desired wavelength across the AUC cell. Matched surfactant solutions were used as the reference. All measurements were conducted at a fixed wavelength of 423 ± 2 nm and temperature of 20 ± 0.5 °C (uncertainties in wavelength and temperature are the instrumental specifications). Generally, a radial scan for each cell was recorded every 5 min. Typical data sets covering the entire sedimentation process included between 85 scans and 190 scans, depending on the density difference, the viscosity of the medium, and the tube length (as shorter SWCNTs take longer to sediment and thus are measured for a longer time). Viscosities and densities of the DOC and DOC−iodixanol solutions were measured independently with an Anton Parr 5000 M densitometer/Lovis ME viscometer combination instrument at 20 °C. In some cases, viscosities and densities for intermediate compositions were linearly interpolated between measured H_2O−surfactant and D_2O−surfactant values. Density and viscosity values were directly measured for each parent solution diluted to form the final solutions of the various combinations of isotopes, surfactants, and iodixanol.

Sedimentation data were analyzed with the software package SEDFIT(version 12p44), which includes the recently reported correction for an instrumental time-stamping issue.[29] Further information about the data analysis and the procedure to measure the density of DOC-SWCNTs is provided in the Supporting Information.

RESULTS AND DISCUSSION

An ideal model colloidal rod system consists of several samples whose constituent particles are uniform in density, diameter, and rigidity, but in which the aspect ratio of particles varies from sample to sample solely due to changes in the length distribution, and that cover a wide range of aspect ratios. Below, we will present how the samples of SWCNTs were prepared and detail why the samples in this work are a good model system to test the accuracy of hydrodynamic models. Subsequently, the predictions from different hydrodynamic models are compared first on their ability to fit the measured sedimentation coefficient set using physically reasonable hydrodynamic parameters and second on their ability to reproduce the entirety of the length distributions independently measured by AFM. Lastly, the relative advantages of determining particle length distributions from sedimentation velocity experiments as compared to other techniques will be presented.

DOC-SWCNTs as Model Rigid Rods. Initial suspensions of SWCNTs contain species that differ in density, length, and state of aggregation. Therefore, for effective comparison of the experimental and theoretical hydrodynamics, rigorous sample preparation was performed. Two SWCNT powders, synthesized by laser ablation and arc-discharge methods (average diameters of approximately 1.35 and 1.5 nm, respectively), were separately dispersed by sonication in sodium deoxycholate (DOC) solution and centrifuged to remove bundles and impurities such as amorphous carbon and catalyst nanoparticles. In addition to individualizing the SWCNTs, however, sonication cuts some of the SWCNTs, affecting the length distribution[30] and enabling filling of the SWCNT core with water through the open ends.[28] Consequently, initial dispersions were significantly polydisperse in density (empty vs filled) and length. A published protocol, exploiting the difference in buoyancy of empty and water-filled SWCNTs, was used to isolate the empty (closed end) SWCNTs.[28] The empty SWCNTs were then length-sorted using size-exclusion chromatography[8] to produce 13 fractions with mass-average lengths between 758 and 68 nm as measured by AFM. These samples were used for AUC experiments.

SWCNT dispersions are often assessed through spectroscopy for properties such as purity, diameter distribution, and dielectric environment. Figure 1a shows the visible and NIR absorption spectra of the initial arc sample and the daughter empty and water-filled SWCNT dispersions. The distribution of peaks (and intensity) indicates that the fractions contain individualized SWCNTs in both the empty and filled fractions.[31] The sharper features and relative blue-shifts of the optical transition peak locations in the empty SWCNT sample, in comparison to the water-filled SWCNT fraction, are known solvatochromic effects;[28,32] this is a consequence of the lower effective dielectric constant the empty SWCNTs experience from having (high dielectric constant) water present only on the exterior of the carbon shell and not interior as well.

Figure 1b shows the spectra of the final empty SWCNT samples after length separation by size-exclusion chromatography. The common distribution of optical transitions, which are a unique property for each SWCNT species, indicates that while multiple SWCNT species are present in the sample, the diameter distribution is constant across the length fractions.[33] Based on (*n*,*m*) assignments from the optical transitions,[33,34] the average diameters for the particular samples used here are

dx.doi.org/10.1021/la404892k | *Langmuir* 2014, 30, 4895−4904

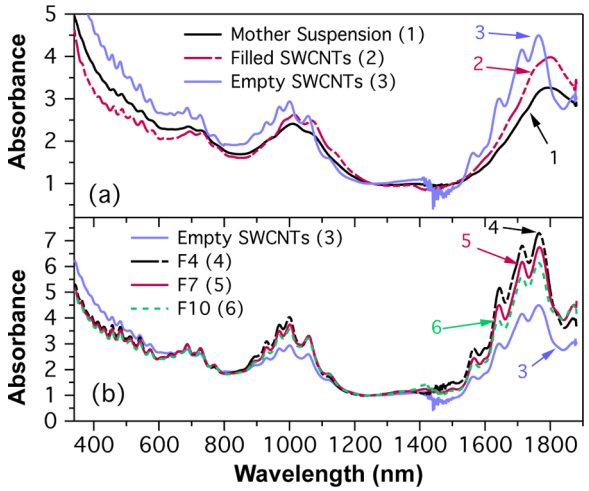

Figure 1. UV/vis/NIR absorption spectra of arc-SWCNTs probing the E_{11} (1500−1900 nm), E_{22} (800−1200 nm), and E_{33} (400−600 nm) transitions of s-SWCNTs and M_{11} (600−800 nm) transitions of m-SWCNTs. (a) Comparison of spectra from the mother suspension (1) to samples after sorting by density, filled (2) and empty (3) SWCNTs. (b) Spectra from empty SWCNTs (3) and samples after sorting by length, F4 (4), F7 (5), and F10 (6).

estimated at 1.48 nm for the arc-SWCNT and 1.33 nm for the laser-SWCNTs (with 177.2 and 159.6 carbon atoms/nm, respectively, based on averaging the structures of the 12 most likely nanotube (*n*,*m*) species).[35] Of additional note is that the peak-to-baseline ratios are enhanced, and similar for the length-sorted populations. This is due to the removal of small (<10 nm) non-nanotube impurities that remain after the empty−filled separation; the length separation additionally removes all of the density modifying agent and ensures all fractions are dispersed in an identical solution environment.

The high quality of the samples indicated by the spectroscopic results is further corroborated by AFM images of the samples. Example images for an intermediate length fraction, F8, for both diameter SWCNT populations are shown in Figure 2. These images (images from other fractions are shown in the Supporting Information) show relatively monodisperse and rigid SWCNTs deposited on the wafer surface as individual tubes with minimal aggregation. Cross-section heights across individual SWCNTs were consistent with single tube diameters. Although a small fraction of tubes appear slightly twisted, it is unclear if this is a reflection of limitations in the separation procedure or a consequence of the drying step during sample preparation, which is known to be able to produce such effects.

Length distributions were created by measuring lengths of SWCNTs from the images and constructing histograms; detailed statistics for each population are reported in the Supporting Information. The resulting length distributions for all the fractions of both arc- and laser-SWCNTs were narrow and show a monotonic change in the average and mode length with fraction number, similar to the previous demonstration of SEC separation.[8] In sum, the UV-vis-NIR spectroscopy and AFM characterization confirm the first two requirements for use as model rodlike particles: that the length-sorted fractions for the arc- or laser-SWCNTs have different (and narrow) length distributions of well-dispersed SWCNTs and that the diameter distribution is consistent across the fractions.

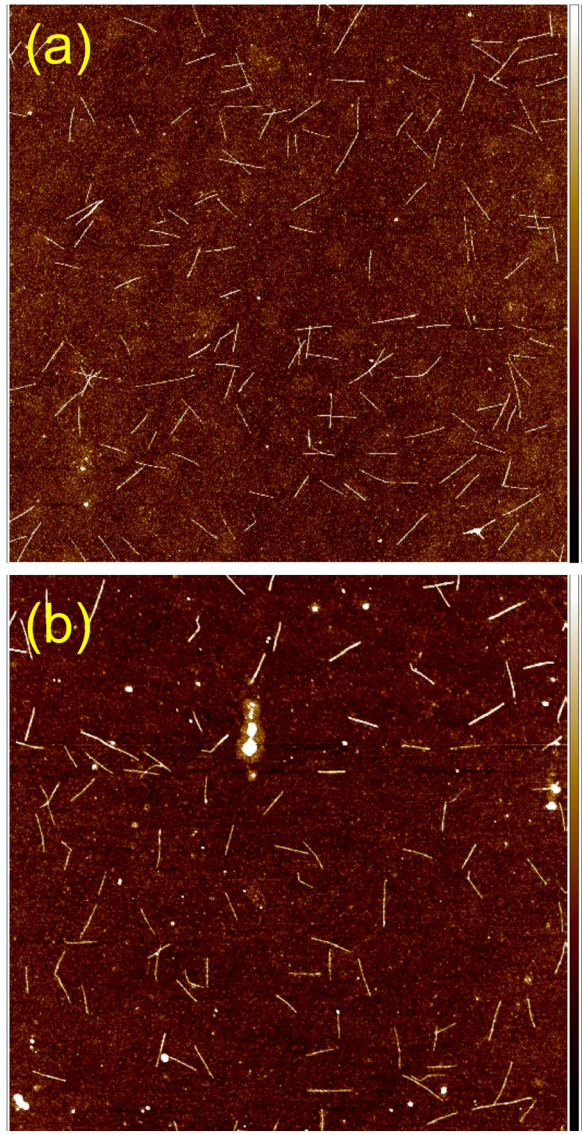

Figure 2. AFM images of SWCNTs from F8 of the (a) arc and (b) laser samples. The size of the images are 4 μm × 4 μm, whereas the color bars represent the height scales, which are −1 to 1.6 nm (arc) and −0.8 to 1.4 nm (laser).

Each doubly sorted sample from both the arc and laser-SWCNT populations was characterized by AUC. Figure 3 shows a set of typical absorbance scans from a sedimentation velocity experiment on fraction 7 (F7). The speed and shape of the sedimentation boundary, defined by the depletion of particles from the inner radius of the solution volume, depend on the size, shape, and buoyancy of the particles. Through a mass balance, the transient transport of dilute and non-interacting species in a sector-shaped cell is governed by the Lamm equation

$$\frac{\partial c}{\partial t} = \frac{1}{r}\frac{\partial}{\partial r}\left[\left(D\frac{\partial c}{\partial r} - \omega^2 sr\right)r\right] \quad (1)$$

where c is the concentration at radial position r and time t; D is the diffusion coefficient. The sedimentation coefficient, s, is the particle velocity normalized by the centrifugal acceleration. Considering that particles in the nanoscale reach terminal

dx.doi.org/10.1021/la404892k | *Langmuir* 2014, 30, 4895−4904

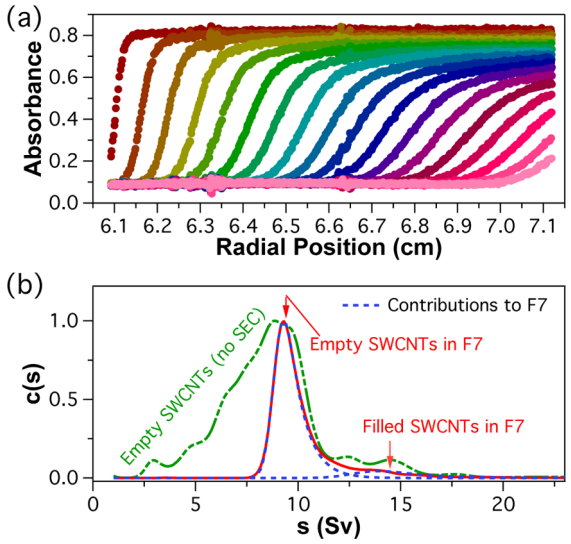

Figure 3. (a) Absorbance as a function of radial position and time during a sedimentation velocity experiment at 25 000 rpm for F7. The absorbance was measured at 423 nm, and the time interval between scans in the figure is 25 min (every fifth scan). (b) Comparison of the sedimentation coefficient distributions, $c(s)$, from the empty SWCNTs and F7 (with spectra 3 and 5 in Figure 1). The blue dashed lines are deconvoluted contributions of the empty and concomitant water-filled SWCNTs in F7.

velocity almost instantaneously ($Re \sim 10^{-7}$), s can be written as the result of a time-independent force balance on a particle

$$s \equiv \frac{u}{\omega^2 r} = \frac{V_p(\rho_p - \rho_s)}{f} \tag{2}$$

where ρ_p and ρ_s are the particle and solvent densities, V_p is the particle volume, and f is the friction coefficient. Therefore, s is a function of the size and density of the particle as well as the friction coefficient and consequently the shape of the particle. As no analytical solution exists for the Lamm equation, solutions to eq 1 were found numerically using the software SEDFIT.[36,37] SEDFIT identifies the most likely values of s present in the experimental data, the relative weight of those values, and performs regularization to find the distribution of sedimentation coefficients, $c(s)$, that are equally likely to generate a given set of sedimentation profiles. Exhaustive details of the fitting in SEDFIT are provided in the Supporting Information. The rotational Péclet (r-*Pe*) number and particle volume fractions were in the low r-*Pe* number and the dilute regimes, respectively. r-*Pe* values (for long to short fractions) ranged from ≈0.01 to 0.0001. Initial particle volume fractions (due to radial dilution these values only decrease with time) were ≈0.003−0.007 (long to short fractions), at most reaching ≈50% of overlap (using the spherical volume swept by the rotating SWCNT) for the longest two fractions and substantially lower (<25% to < 1%) for the shorter ones. Experimentally, we confirmed these limits by the measurement of sedimentation coefficients distributions for the fractions over a 32× change in centrifugal acceleration (7 to 40 krpm) and found the distributions to be equivalent. This result confirmed that the friction coefficient is not rate dependent and thus rotationally averaged at the measured conditions.

For an ensemble of rods of uniform density, the width of the $c(s)$ is a consequence of length polydispersity. Thus, the significant narrowing (fwhm ≈ 1 Sv) of the length sorted populations compared to the empty parent (fwhm ≈ 4 Sv) is visible in Figure 3b; it should be noted that the empty parent $c(s)$ is itself substantially narrower than an unsorted sample.[38] Unfortunately, because the empty-filled separation is not 100% efficient, the length sorted empty SWCNT populations still contain a small amount of water-filled SWCNTs (of the same length distribution), which produces a small shoulder peak at greater s values in the sedimentation coefficient distribution. To separate the contributions of the two components for comparison to the hydrodynamic models, the $c(s)$ distributions determined through SEDFIT were decomposed into a combination of two bimodal right-skewed Gaussian functions (Supporting Information) of similar shape but different peak positions, after confirming the identity of the two populations via density contrast measurements (*vida infra*). An example of the extracted contributions is shown in Figure 3b for fraction F7 by the blue dashed curves.

Substantial density contrast measurements (below and in Supporting Information) were performed on length fractions from each of the arc- and laser-SWCNT samples to explicitly measure the anhydrous and hydrated densities of both the empty and filled component peaks. These measurements confirmed that the shoulder peaks at greater s display density values consistent with water-filled SWCNTs, allowing for the decomposition of the contributions to the $c(s)$ described above. These experiments also critically provide both a density value and an anhydrous radial radius (R_{AH}) for the anhydrous SWCNT−surfactant complex, and a hydrated radial radius, independent of any hydrodynamic factors (R_{Hyd}). With these independently measured densities, and the determined $c(s)$ distributions for the empty SWCNT length fractions, we know all of the factors in eq 2 except for the shape factor and can proceed to make comparisons to comparing against the hydrodynamic models. Before demonstrating the validity of the advanced models to describe the SWCNT fractions, however, it is worth being explicit in the description of the DOC−SWCNT complex, its respective hydration layer, and the relation to the hydrodynamic factors.

Structural Description of Colloidal DOC−SWCNTs. SWCNTs suspended in water with the aid of DOC have a complex interface with a portion of the tube covered by surfactant molecules and a concomitant hydration shell due to the correlation/bonding of water molecules to DOC. Using a shell model and a mass balance to interpret the measured densities from the density contrast measurements, one can calculate minimal radial R_{AH} (accounting for the mass of the SWCNTs and adsorbed DOC) and a minimal radial R_{Hyd} (containing sufficient water to account for the density difference between hydrated and anhydrous densities; see Supporting Information and refs 39 and 40 for more details). A schematic of the shell model labeling the different important radii is shown in Figure 4A. Note that the mass of the surfactant and water components can be distributed in any manner within the annular volume surrounding the CNT without affecting the measured density; a "layer-cake" model purely simplifies the presentation. The graphical determination of the anhydrous and hydrated densities for the arc-SWCNTs using H_2O to D_2O variation, or the addition of a nonadsorbing density modifying agent (iodixanol), respectively, is shown in Figure 5.

The results from the calculations and the values of the relevant parameters employed are compiled in Table 1. The values of R_{AH} for both SWCNT samples are physically reasonable when one considers the molecular dimensions of

dx.doi.org/10.1021/la404892k | *Langmuir* 2014, 30, 4895−4904

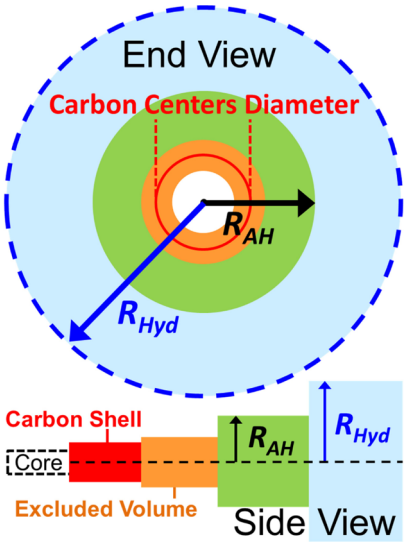

Figure 4. Shell model schematic of a nanotube in solution, end and side views, showing the various layers and radii definitions described in the text.

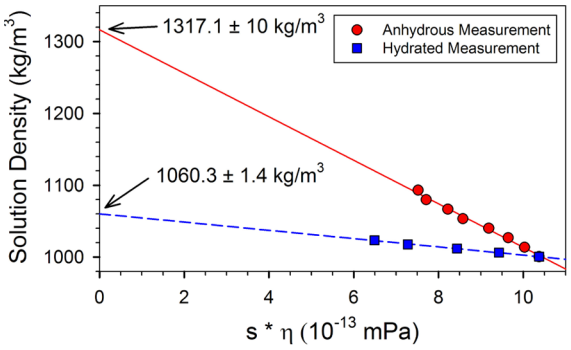

Figure 5. Determination of anhydrous and hydrated densities for the arc-SWCNTs as given by the *y*-intercept extrapolated from the change in *s*, for the same SWCNTs, in different density media. Plotted values include the correction for viscosity (η). The anhydrous density was measured in mixtures of H_2O–D_2O ranging in concentration from 0 to 87.5% D_2O; the hydrated density was measured in solutions of iodixanol (1, 2, 3, and 4 wt %).

Table 1. Relevant Parameters for the Calculation of R_{AH} and R_{Hyd}

parameter	arc-SWCNTs	laser-SWCNTs
density of solution (kg/m^3)	1000.40	1000.40
viscosity of solution (mPa·s)	1.0567	1.0567
specific volume of DOC (cm^3/g)	0.7734	0.7734
avg SWCNT species (C atoms/nm)	177.2	159.6
avg SWCNT diameter, d_{c-c} (nm)	1.48	1.33
anhydrous density (kg/m^3)	1317.1 ± 9.6	1352.8 ± 16.8
hydrated density (kg/m^3)	1060.3 ± 1.4	1071.2
R_{AH} (nm)	1.51 ± 0.45	1.38 ± 0.20
R_{Hyd} (nm)	3.48 ± 1.0	3.07 ± 0.55

the DOC molecules. DOC molecules can be geometrically approximated by ellipsoids with semiaxes of 4 and 21 Å.[41] Unlike for the small diameter (6,5) SWCNT, the surfactant shell seems to be formed on average by a single layer of DOC molecules.[40] The primary uncertainties in the radii values evolve from closeness of the average anhydrous density value to the measured DOC density and the calculated density of the empty SWCNT structure for some (*n*,*m*) species. Species sorting, to reduce the ambiguity of averaging over multiple (*n*,*m*) structures, should allow for dramatic reduction in the uncertainty values, but it is beyond the scope of this contribution.

The values of ρ_{AH} and the mass balance reveal that DOC–SWCNTs are substantially hydrated. The level of hydration in proteins is usually described by the parameter δ, which is defined as grams of water per gram of proteins.[42] A similar definition can be adopted to describe the hydration of SWCNTs, where δ can be defined as grams of water per gram of DOC–SWCNTs. For both samples $\delta \approx 3.2$, which is large but not outlandish compared to the hydration of proteins ($\delta \approx 0.3$) considering that the empty DOC–SWCNTs have a much larger surface area per unit of mass. In addition, strong hydration is expected on DOC–SWCNTs due to the chemical characteristics of DOC. DOC molecules likely assemble on SWCNTs with the hydrophobic face aligned with the SWCNT while exposing the hydrophilic face to water. The hydrophilic face contains one charged group and two hydroxyl groups.

One more important remark needs to be made. The values of R_{AH} and R_{Hyd} are the *minimum values* possible given the measured mass of a DOC–SWCNT. The smooth cylinder model assumes the surfactant molecules to be tightly packed and evenly distributed on the surface of the SWCNTs. The friction coefficient likely has a contribution from the surface roughness of the particles similar to what happen in proteins.[43] Consequently, and crucially, values of radial hydrodynamic radius, R_{HDM}, from theory should not be lower than R_{Hyd}.

Comparison to Hydrodynamic Models Predictions for Rigid Rods. The expressions considered (Supporting Information) in this work are consistent in that the sedimentation coefficient of a smooth and long cylinder should be approximately a logarithmic function of length. For example, from the slender body theory of Batchelor[5] the orientation averaged translational friction coefficient, obtained by taking the harmonic mean of the longitudinal and orthogonal friction components, can be calculated from the following approximate expression

$$f = 6\pi\eta L \frac{Y^3 + 0.614Y^2 + 0.638Y + 0.0135}{2Y^4 + 0.614Y^3 + 0.544Y^2 - 0.136} \quad (3)$$

in which η is the viscosity of the solvent and Y is defined as $\ln(L/R_{HDM})$. Consequently, *s* values plotted versus the mass-averaged AFM determined length should, to first order, form a logarithmic slope from the approximate functionality (combining eqs 2 and 3) of $\ln(L/R_{HDM})$. Plotting the average *s* value for the empty components versus the mass-averaged length for each fraction in Figures 6a and 6b (arc and laser samples, respectively), this qualitative logarithmic functionality is indeed immediately apparent.

Quantitative comparison with the hydrodynamic data was conducted by fitting the data in Figure 6 floating solely the value of R_{HDM}. These values are reported in Table 2. As stated earlier, this is possible using the independently determined (and length independent) R_{AH} values for the arc and laser fractions calculated from the density measurements and the known (measured) solution and surfactant parameters. Nanotube geometrical factors were calculated using commercial software. The comparison point for the best fit value from each hydrodynamic model is then the independently determined

dx.doi.org/10.1021/la404892k | *Langmuir* 2014, 30, 4895–4904

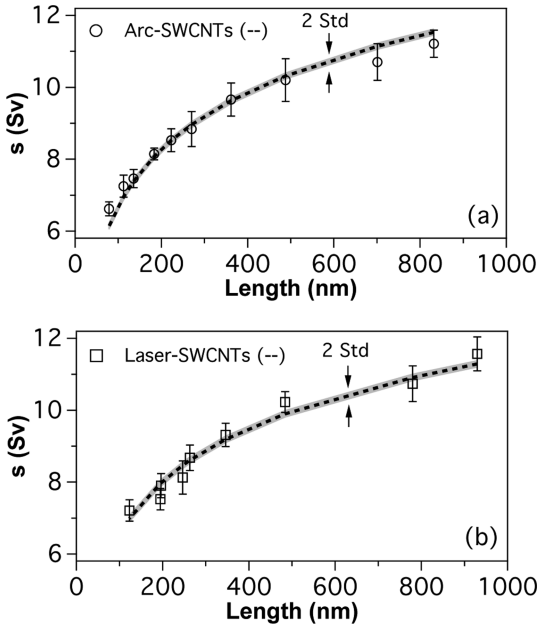

Figure 6. Average sedimentation coefficient (s) is a logarithmic function of the mass-averaged length measured by AFM for the arc (a) and laser (b) samples. The error bars represent the fwhm of the sedimentation distribution peaks, whereas the dashed lines are best fits to the data using Batchelor's expression and R_{HDM} as a fitting parameter. The shaded regions indicate where the fits fall within two standard deviation (Std) of the best fit for R_{HDM}.

Table 2. Hydrodynamic Radii Calculated from the Sedimentation Coefficient and Average Length of Each Fraction (Figure 6)[a]

	R_{HDM} (nm)	
expression	arc	laser
Batchelor[b]	1.44 ± 0.06	1.09 ± 0.12
Broesma	2.84 ± 0.14	2.49 ± 0.10
Batchelor	3.77 ± 0.14	3.22 ± 0.14
Mansfield–Douglas	3.53 ± 0.13	3.01 ± 0.13
Aragon–Flamik	3.54 ± 0.13	3.02 ± 0.12
mass balance	3.48 ± 1.00	3.07 ± 0.55

[a]The friction coefficient was calculated using the expressions reported by Batchelor, Broersma, Aragon–Flamik, and Mansfield–Douglas and using the values of R_{AH} calculated through the mass balance, 1.51 ± 0.45 and 1.38 ± 0.20 nm for the arc and laser samples. [b]Only the leading term of the complete expression was used in the calculation.

(from the anhydrous and hydrated densities (Supporting Information)) hydrated radius (R_{Hyd}).

As R_{Hyd} represents a minimal radius of correlated water, R_{HDM} cannot reasonably be smaller than this value. This condition is our first comparison criterion. Values of R_{HDM} (Table 2) for Broersma's relation and the Batchelor's leading term expression fail this criteria for the best fit value. As discussed by Batchelor,[5] these expressions include only the first- and second-order terms of a matched asymptotic expansion limiting their accuracy. Consequently, as remarked by Mansfield and Douglas, the Broersma's expression deviates significantly from the "exact" value at aspect ratios below 50 and in our case leads to a nonphysical R_{HDM} best fit value for the broad range of experimental aspect ratios. In contrast, the more elaborate models, such as the expressions of Batchelor or Mansfield–Douglas, impressively describe the experimental data (Table 2), with best fit values for R_{HDM} indistinguishable from or larger than R_{Hyd}. Since assigning the shear plane at the interface between the bound volume of surfactant and water and the bulk solution is reasonable, this is a direct validation that these hydrodynamic equations accurately reflect the friction of the nanotubes as rods over a wide range of aspect ratios.

The ultimate test for the accuracy of the expressions, however, is the ability to reproduce the shape, mode, and width of the actual length distribution for each sample from its respective $c(s)$. A comparison of the length distributions measured by AFM and the calculated distribution from AUC, assigning R_{HDM} equal to R_{Hyd} from the mass balance, is shown in Figure 7. The reproduction of the shape, mode, and width of the distributions by the Batchelor expression as well as the expressions from numerical calculations (Mansfield–Douglas and Aragon–Flamik) is remarkable. Note how the length distributions derived from sedimentation velocity become progressively more accurate with the inclusion of additional terms in the matched asymptotic expansions from slender body theory. To predict the friction coefficient of rigid SWCNTs, users of slender body theory should thus be careful to use sufficiently advanced hydrodynamic models in their calculations, especially for particles not in the large Y limit.

Determining Particle Length Distributions of SWCNTs through Sedimentation Velocity Experiments. Impressively, it is possible to extract length distributions of SWCNTs from sedimentation velocity experiments without a single fitting parameter (see Figure 7) using the Batchelor, Mansfield–Douglas, or Aragon–Flamik (Supporting Information) hydrodynamic models. To further explore the use of sedimentation velocity experiments as a method for extracting the length distribution of rods, we now compare the distributions predicted from the $c(s)$ distributions using the Mansfield–Douglas model for all the arc-SWCNTs (larger diameter) fractions. This comparison across the entire range of different aspect ratio samples is shown in Figure 8, again using the assumption that the measured $R_{Hyd} = R_{HDM}$. As seen in the figure, the AUC derived distributions well reproduce the shape of the AFM histograms across the entire range of aspect ratios for the arc-SWCNTs, albeit with a some small mismatches in the modes for the longest and shortest fractions. In the case of the laser-SWCNTs (Supporting Information), the agreement between the sedimentation data and the AFM data is also impressive, showing superb agreement for almost all fractions. The AUC data in general are able to reproduce the back tail but fails to reproduce the front tail, perhaps due to smoothing from decomposing the empty and filled populations or from the use of the average density for all nanotubes whereas the actual density and geometry vary across (n,m) species. As would be expected, the predicted length distributions vary only slightly when using expressions from the numerical methods of Mansfield–Douglas or Aragon–Flamik instead of the Batchelor expression. Although visually the different expressions may provide slightly better or worse fits, we cannot clearly differentiate between them with current uncertainties. A statistical comparison of the distribution average, mode, and width is presented in the Supporting Information for each fraction. The good agreement demonstrates that sedimentation velocity experiments, along with correctly measured parameters (R_{AH} and R_{Hyd}), can produce statistically realistic length distributions of SWCNTs. That AUC data can reproduce the length distribution of particles from only measurable

dx.doi.org/10.1021/la404892k | Langmuir 2014, 30, 4895–4904

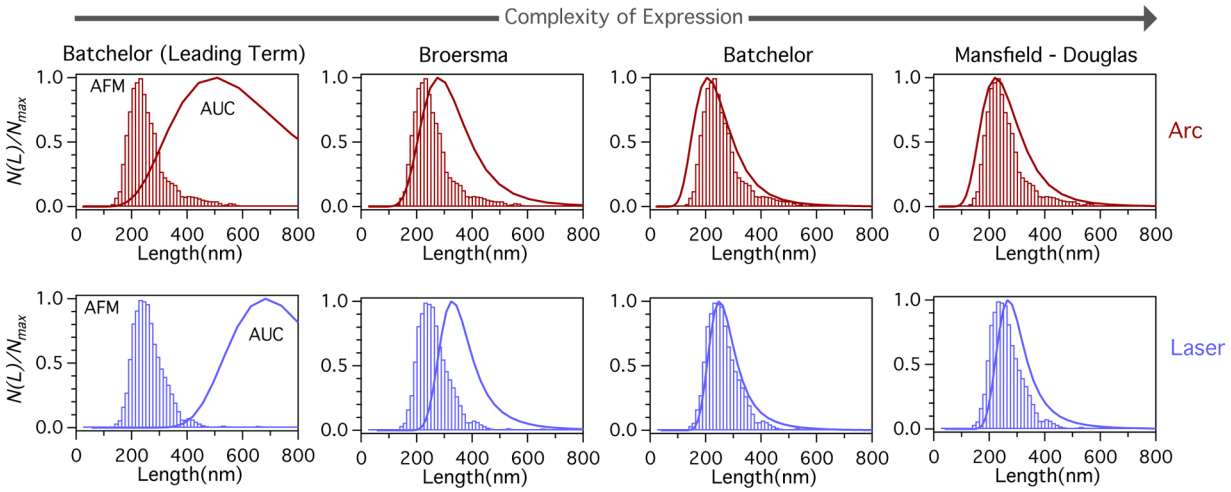

Figure 7. Normalized length distributions, $N(L)/N_{max}$, measured by AFM and AUC for F8 in both the arc and laser samples. AUC distributions calculated through the Mansfield−Douglas and the Batchelor expressions reproduce the AFM distributions. In contrast, the expressions by Batchelor (leading term) and Broersma are not accurate enough to reproduce the AFM distributions. Lengths were calculated from the sedimentation coefficients using R_{AH} and with R_{HDM} equal to R_{Hyd}.

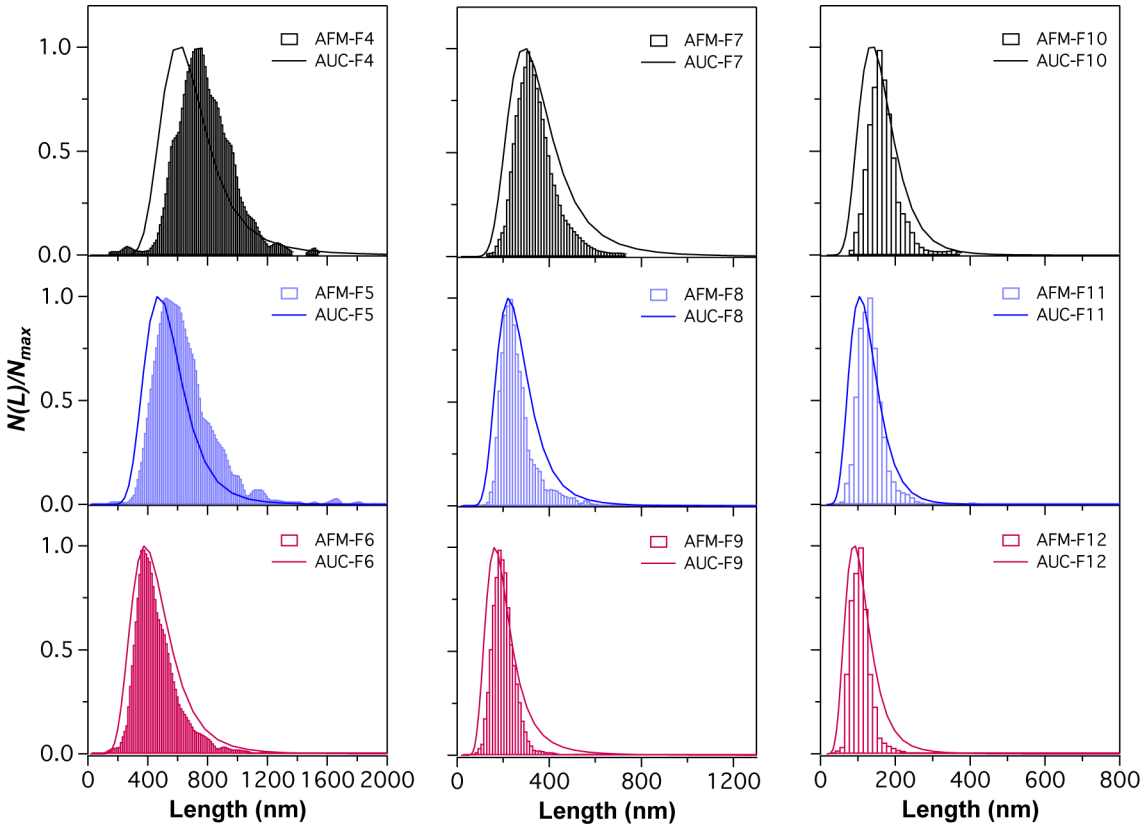

Figure 8. Normalized length distributions, $N(L)/N_{max}$, measured by AFM and AUC for all length-sorted fractions of arc-SWCNTs. The AUC length distributions were calculated from the sedimentation coefficients using the Mansfield−Douglas expression, R_{AH} and R_{HDM} equal to R_{Hyd}. Notice that horizontal scale changes for each column.

parameters over such a wide range in aspect ratio is outstanding.

Given the demonstrated ability of the method to reproduce length distributions, sedimentation velocity experiments have the additional advantage over counting methods such as AFM that an ensemble of billions of particles are measured in a single experiment. Assuming experiments are handled appropriately to minimize noise and error, a sample size statistically representative of the entire sample should be measured in a single shot, as opposed to counting methods where distribution tails can be easily overlooked. Additionally, in sedimentation velocity experiments, the particles are measured in the liquid state, avoiding complications and possible biases generated from any deposition and drying process. In comparison to alternative methods where length distributions are determined by measuring the diffusivity (or alignment) of particles in

dx.doi.org/10.1021/la404892k | Langmuir 2014, 30, 4895−4904

quiescent (flow) conditions,[24,26] the measurements here were performed without a single direct fitting parameter, and one can assume a uniform (no-shear) flow field. Other advantages include benefiting from the high signal-to-noise ratio detection (absorbance) even at low volume fractions accorded by the large intrinsic nanotube absorbance cross sections, and the small size of the SWCNTs keeps the *Re* and r-*Pe* numbers small enough to exclude complicating factors. While AUC has relative disadvantages to other techniques (high cost, experimental complexity, need for high precision density values), beyond research applications AUC has high promise for specific applications such as certification of nanoparticle-based medicine lots, where the resolution power of the distribution is important and constant density parameters would ease implementation. Areas to be improved upon would include narrowing the SWCNT populations further to improve accuracy for the geometric values and usable volume fraction range and comparison to other techniques for improved qualification of relative advantages and weaknesses.

CONCLUSIONS

In summary, doubly sorted SWCNTs were used as model rodlike particles to validate expressions for the friction coefficients from hydrodynamic theory as determined by direct comparison to independently measured physical parameters and the ability to independently reproduce length distributions measured by AFM. To our knowledge, this the first time in that the hydrodynamic theory of rigid-rod-like particles has been experimentally probed with a model system spanning an order of magnitude in aspect ratio: <50 to >400. We anticipate that SWCNTs will provide an exceptional model particle for further direct probing of hydrodynamic phenomenon at the nanoscale.

ASSOCIATED CONTENT

Supporting Information

Further details on methods and data analysis as well as the statistical information for length distributions measured by AFM and AUC. This material is available free of charge via the Internet at http://pubs.acs.org.

AUTHOR INFORMATION

Corresponding Author

*E-mail: Jeffrey.fagan@nist.gov (J.A.F.).

Notes

The authors declare no competing financial interest.

REFERENCES

(1) Jeffery, G. B. *Proc. R. Soc. London, Ser. A* **1922**, *102*, 161−179.
(2) Cademartiri, L.; Bishop, K. J. M.; Snyder, P. W.; Ozin, G. A. Using Shape for Self-Assembly. *Philos. Trans. R. Soc. A* **2012**, *370*, 2824−2847.
(3) Rodríguez-Fernández, J.; Pérez Juste, J.; Liz-Marzan, L. M.; Lang, P. Dynamic Light Scattering of Short Au Rods with Low Aspect Ratios. *J. Phys. Chem. C* **2007**, *111*, 5020−5025.
(4) Martchenko, I.; Dietsch, H.; Moitzi, C.; Schurtenberger, P. Hydrodynamic Properties of Magnetic Nanoparticles with Tunable Shape Anisotropy: Prediction and Experimental Verification. *J. Phys. Chem. B* **2011**, *115*, 14838−14845.
(5) Batchelor, G. K. Slender-Body Theory for Particles of Arbitrary Cross-Section in Stokes Flow. *J. Fluid Mech.* **1970**, *44*, 419−440.
(6) Mansfield, M. L.; Douglas, J. F. Transport Properties of Rodlike Particles. *Macromolecules* **2008**, *41*, 5422−5432.
(7) Aragon, S. R.; Flamik, D. High Precision Transport Properties of Cylinders by the Boundary Element Method. *Macromolecules* **2009**, *42*, 6290−6299.
(8) Khripin, C. Y.; Tu, X.; Heddleston, J. M.; Silvera-Batista, C.; Hight Walker, A. R.; Fagan, J.; Zheng, M. High-Resolution Length Fractionation of Surfactant-Dispersed Carbon Nanotubes. *Anal. Chem.* **2013**, *85*, 1382−1388.
(9) Fakhri, N.; MacKintosh, F. C.; Lounis, B.; Cognet, L.; Pasquali, M. Brownian Motion of Stiff Filaments in a Crowded Environment. *Science* **2010**, *330*, 1804−1807.
(10) Tsyboulski, D. A.; Bachilo, S. M.; Kolomeisky, A. B.; Weisman, R. B. Translational and Rotational Dynamics of Individual Single-Walled Carbon Nanotubes in Aqueous Suspension. *ACS Nano* **2008**, *2*, 1770−1776.
(11) Silvera-Batista, C. A.; Ziegler, K. J. Swelling the Hydrophobic Core of Surfactant- Suspended Single-Walled Carbon Nanotubes: A SANS Study. *Langmuir* **2011**, *27*, 11372−11380.
(12) Fagan, J. A.; Becker, M. L.; Chun, J.; Nie, P.; Bauer, B. J.; Simpson, J. R.; Hight- Walker, A.; Hobbie, E. K. Centrifugal Length Separation of Carbon Nanotubes. *Langmuir* **2008**, *24*, 13880−133889.
(13) Donkai, N.; Inagaki, H.; Kajiwara, K.; Urakawa, H. Dilute Solution Properties of Imogolite. *Macromol. Chem. Phys.* **1985**, *186*, 2623−2638.
(14) Tirado, M. M.; Martínez, C. L.; García de la Torre, J. Comparison of Theories for the Translational and Rotational Diffusion Coefficients of Rod-like Macromolecules. Application to Short DNA Fragments. *J. Chem. Phys.* **1984**, *81*, 2047−2052.
(15) Mukhija, D.; Solomon, M. J. Translational and Rotational Dynamics of Colloidal Rods by Direct Visualization with Confocal Microscopy. *J. Colloid Interface Sci.* **2007**, *314*, 98−106.
(16) Han, Y.; Alsayed, A.; Nobili, M.; Yodh, A. Quasi-Two-Dimensional Diffusion of Single Ellipsoids: Aspect Ratio and Confinement Effects. *Phys. Rev. E* **2009**, *80*, 011403.
(17) Santos, N. C.; Castanho, M. A. Teaching Light Scattering Spectroscopy: the Dimension and Shape of Tobacco Mosaic Virus. *Biophys. J.* **1996**, *71*, 1641−1650.
(18) Straus, S.; Scott, W.; Symmons, M.; Marvin, D. On the Structures of Filamentous Bacteriophage Ff (fd, f1, M13). *Eur. Biophys. J.* **2008**, *37*, 521−527.
(19) Wierenga, A. M.; Philipse, A. P. Low-Shear Viscosities of Dilute Dispersions of Colloidal Rodlike Silica Particles in Cyclohexane. *J. Colloid Interface Sci.* **1996**, *180*, 360−370.
(20) Dogic, Z.; Fraden, S. Ordered Phases of Filamentous Viruses. *Curr. Opin. Colloid Interface Sci.* **2006**, *11*, 1−9.
(21) Tracy, M. A.; Pecora, R. Dynamics of Rigid and Semirigid Rodlike Polymers. *Annu. Rev. Phys. Chem.* **1992**, *43*, 525−557.
(22) Barry, E.; Beller, D.; Dogic, Z. A Model Liquid Crystalline System Based on Rodlike Viruses with Variable Chirality and Persistence Length. *Soft Matter* **2009**, *5*, 2563−2570.
(23) Planken, K. L.; Cölfen, H. Analytical Ultracentrifugation of Colloids. *Nanoscale* **2010**, *2*, 1849.
(24) Streit, J. K.; Bachilo, S. M.; Naumov, A. V.; Khripin, C.; Zheng, M.; Weisman, R. B. Measuring Single-Walled Carbon Nanotube Length Distributions from Diffusional Trajectories. *ACS Nano* **2012**, *6*, 8424−8431.
(25) Casey, J. P.; Bachilo, S. M.; Moran, C. H.; Weisman, R. B. Chirality-Resolved Length Analysis of Single-Walled Carbon Nanotube Samples through Shear-Aligned Photoluminescence Anisotropy. *ACS Nano* **2008**, *2*, 1738−1746.
(26) Reuel, N. F.; Dupont, A.; Thouvenin, O.; Lamb, D. C.; Strano, M. S. Three-Dimensional Tracking of Carbon Nanotubes within Living Cells. *ACS Nano* **2012**, *6*, 5420−5428.
(27) Certain equipment, instruments or materials are identified in this paper in order to adequately specify the experimental details. Such identification does not imply recommendation by the National Institute of Standards and Technology nor does it imply the materials are necessarily the best available for the purpose.

(28) Fagan, J. A.; Huh, J. Y.; Simpson, J. R.; Blackburn, J. L.; Holt, J. M.; Larsen, B. A.; Walker, A. R. H. Separation of Empty and Water-Filled Single-Wall Carbon Nanotubes. *ACS Nano* **2011**, *5*, 3943−3953.
(29) Zhao, H.; Ghirlando, R.; Piszczek, G.; Curth, U.; Brautigam, C. A.; Schuck, P. Recorded Scan Times Can Limit the Accuracy of Sedimentation Coefficients in Analytical Ultracentrifugation. *Anal. Biochem.* **2013**, *437*, 104−108.
(30) Pagani, G.; Green, M. J.; Poulin, P.; Pasquali, M. Competing Mechanisms and Scaling Laws for Carbon Nanotube Scission by Ultrasonication. *Proc. Natl. Acad. Sci. U. S. A.* **109**, 11599−11604.
(31) O'Connell, M.; Bachilo, S.; Huffman, C.; Moore, V.; Strano, M.; Haroz, E.; Rialon, K.; Boul, P.; Noon, W.; Kittrell, C.; Ma, J.; Hauge, R.; Weisman, R.; Smalley, R. Band Gap Fluorescence from Individual Single-Walled Carbon Nanotubes. *Science* **2002**, *297*, 593−596.
(32) Silvera-Batista, C. A.; Wang, R. K.; Weinberg, P.; Ziegler, K. J. Solvatochromic Shifts of Single-Walled Carbon Nanotubes in Nonpolar Microenvironments. *Phys. Chem. Chem. Phys.* **2010**, *12*, 6990−6998.
(33) Bachilo, S.; Strano, M.; Kittrell, C.; Hauge, R.; Smalley, R.; Weisman, R. Structure-Assigned Optical Spectra of Single-Walled Carbon Nanotubes. *Science* **2002**, *298*, 2361−2366.
(34) Cambré, S.; Wenseleers, W. Separation and Diameter-Sorting of Empty (End-Capped) and Water-Filled (Open) Carbon Nanotubes by Density Gradient Ultracentrifugation. *Angew. Chem., Int. Ed.* **2011**, *50*, 2764−2768.
(35) Nanotube Modeller, Version 1.7.1; JCrystalSoft, http://www.jcrystal.com.
(36) Schuck, P. Size-Distribution Analysis of Macromolecules by Sedimentation Velocity Ultracentrifugation and Lamm Equation Modeling. *Biophys. J.* **2000**, *78*, 1606−1619.
(37) Brown, P.; Schuck, P. Macromolecular Size-and-Shape Distributions by Sedimentation Velocity Analytical Ultracentrifugation. *Biophys. J.* **2006**, *90*, 4651−4661.
(38) Backes, C.; Karabudak, E.; Schmidt, C. D.; Hauke, F.; Hirsch, A.; Wohlleben, W. Determination of the Surfactant Density on SWCNTs by Analytical Ultracentrifugation. *Chem.—Eur. J.* **2010**, *16*, 13176−13184.
(39) Arnold, M. S.; Suntivich, J.; Stupp, S. I.; Hersam, M. C. Hydrodynamic Characterization of Surfactant Encapsulated Carbon Nanotubes Using an Analytical Ultracentrifuge. *ACS Nano* **2008**, *2*, 2291−2300.
(40) Fagan, J. A.; Zheng, M.; Rastogi, V.; Simpson, J. R.; Khripin, C. Y.; Silvera Batista, C. A.; Hight Walker, A. R. Analyzing Surfactant Structures on Length and Chirality Resolved (6,5) Single-Wall Carbon Nanotubes by Analytical Ultracentrifugation. *ACS Nano* **2013**, *7*, 3373−3387.
(41) Santhanalakshmi, J.; Lakshmi, G.; Aswal, V.; Goyal, P. Small-Angle Neutron Scattering Study of Sodium Cholate and Sodium Deoxycholate Interacting Micelles in Aqueous Medium. *Proc. Indian Acad. Sci.—Chem. Sci.* **2001**, *113*, 55−62.
(42) García de la Torre, J. Hydration from Hydrodynamic. General Considerations and Applications of Bead Modelling to Globular Proteins. *Biophys. Chem.* **2001**, *93*, 159−170.
(43) Erickson, H. P. Size and Shape of Protein Molecules at the Nanometer Level Determined by Sedimentation, Gel Filtration, and Electron Microscopy. *Biol. Proced. Online* **2009**, *11*, 32−51.